Research Articles

Batteries Very Important Paper

How to cite: *Angew. Chem. Int. Ed.* **2020**, *59*, 19311–19319
International Edition: doi.org/10.1002/anie.202009064
German Edition: doi.org/10.1002/ange.202009064

High-Capacity and Stable Li-O$_2$ Batteries Enabled by a Trifunctional Soluble Redox Mediator

Qi Xiong[+], *Gang Huang*[+], *and Xin-Bo Zhang**

Abstract: *Li-O$_2$ batteries with ultrahigh theoretical energy densities usually suffer from low practical discharge capacities and inferior cycling stability owing to the cathode passivation caused by insulating discharge products and by-products. Here, a trifunctional ether-based redox mediator, 2,5-di-tert-butyl-1,4-dimethoxybenzene (DBDMB), is introduced into the electrolyte to capture reactive O_2^- and alleviate the rigorous oxidative environment of Li-O$_2$ batteries. Thanks to the strong solvation effect of DBDMB towards Li^+ and O_2^-, it not only reduces the formation of by-products (a high Li_2O_2 yield of 96.6 %), but also promotes the solution growth of large-sized Li_2O_2 particles, avoiding the passivation of cathode as well as enabling a large discharge capacity. Moreover, DBDMB makes the oxidization of Li_2O_2 and the decomposition of main by-products (Li_2CO_3 and LiOH) proceed in a highly effective manner, prolonging the stability of Li-O$_2$ batteries (243 cycles at 1000 mAh g^{-1} and 1000 mA g^{-1}).*

Introduction

Rechargeable aprotic Li-O$_2$ batteries with ultrahigh theoretical specific energy densities (3460 Wh kg^{-1}), which far exceed those of Li-ion batteries,[1] have aroused worldwide attention.[2] The typical electrochemistry of Li-O$_2$ batteries is based on the reaction between lithium metal and O$_2$ with the formation and decomposition of Li_2O_2 during the discharge and charge processes. There are two pathways for the growth of Li_2O_2 from intermediate O_2^- having been proposed: surface mechanism and solution mechanism.[3] Growth of Li_2O_2, a wide band-gap insulator,[4] on the gas diffusion cathode by surface mechanism will passivate the cathode, thus leads to a low discharge capacity and early death of batteries.[3a] In contrast, the growth of Li_2O_2 by solution mechanism will obtain large-sized Li_2O_2 toroidals with a higher discharge capacity.[3a] Therefore, some solutions have been proposed to promote the Li-O$_2$ batteries discharge in the solution-mediated pathway, so as to unlock their ultrahigh energy densities. Among them, electrolytes with high donor number (DN) or acceptor number (AN), which can increase the solubility of Li^+ or O_2^-, prefer solution mechanism.[3a,5] Protic additives, such as water and phenol, can also trigger solution-mediated pathway by forming hydroperoxide.[3a,6] For O$_2$ reduction redox mediators (RMs), they can catalyze O$_2$ reduction and increase the concentration of O_2^- in solution, resulting in remarkable improvement of discharge capacity.[7] Although the solution mechanism can enlarge specific capacities, the complete decomposition of large-sized Li_2O_2 is really a tough task, due to the fact that the oxygen evolution reaction (OER) takes place at the inner interface of Li_2O_2 and cathode,[8] making the Li_2O_2 far away from cathode leave over.

Recently, OER RMs, a kind of liquid catalysts for facilitating homogenous catalysis, have been developed.[9] Unlike the directly electrochemical oxidation of Li_2O_2 by solid catalyst with charge transfer limitations, RM is firstly oxidized to its oxidation state (RM^+) at the cathode, then, RM^+ diffuses to the vicinity of Li_2O_2 particles to chemically oxidative decomposition of Li_2O_2 with the simultaneous recovery of RM^+ to its reduced form. This chemical oxidation of Li_2O_2 with the help of RM can enlarge the reaction region for Li_2O_2 decomposition and avoid the formation of reactive and defective intermediate, $Li_{2-x}O_2$, as a result, improving the charge efficiency and reducing side reactions to a much low degree.[9g,10]

However, the significance of RMs for promoting the decomposition of Li_2CO_3 and LiOH, main by-products in the operation of Li-O$_2$ batteries, has long been ignored. Despite glyme-based electrolytes are relatively more stable than other electrolytes,[2b,11] they are still susceptible to nucleophilic attack by reduced oxygen species, O_2^-,[12] Li_2O_2,[13] and so on, generating Li_2CO_3 and LiOH and resulting in low Li_2O_2 yield of about 80 %.[14] Besides electrolytes, the usually adopted carbon-based cathodes are also vulnerable to reduced oxygen species, especially O_2^-, easily leading to the generation of a monolayer of Li_2CO_3 at the interface of carbon-Li_2O_2.[13b,15] Since the intrinsic obstacles for oxidization of the redox-inert anions, OH^- and CO_3^{2-}, are large, the electrochemical decomposition of LiOH and Li_2CO_3 is highly energy consumption and much more difficult than that of Li_2O_2.[16] Thus, the presence of LiOH and Li_2CO_3 can severely reduce the

---

[*] Q. Xiong,[+] Prof. X.-B. Zhang
State Key Laboratory of Rare Earth Resource Utilization, Changchun Institute of Applied Chemistry, Chinese Academy of Sciences
Changchun, 130022 (P. R. China)
E-mail: xbzhang@ciac.ac.cn

Q. Xiong[+]
Key Laboratory of Automobile Materials, Ministry of Education, Department of Materials Science and Engineering, Jilin University
Changchun, 130022 (P. R. China)

Prof. X.-B. Zhang
University of Science and Technology of China
Hefei, 230026 (P. R. China)

Dr. G. Huang[+]
Physical Science and Engineering Division, King Abdullah University of Science and Technology (KAUST)
Thuwal, 23955-6900 (Saudi Arabia)

[+] These authors contributed equally to this work.

Supporting information and the ORCID identification number(s) for the author(s) of this article can be found under: https://doi.org/10.1002/anie.202009064.

transport current,[13b,16] resulting in a high charge voltage, which in turn, further exacerbates side reactions. Once the active sites are covered by the gradually accumulated LiOH and Li_2CO_3, the catalytic sites of cathode diminish and the mass and charge transfer will be further limited, which eventually leads to the early death of Li-O_2 batteries. Therefore, in order to prolong the cycling stability of Li-O_2 batteries, a RM that only active for Li_2O_2 cannot meet these requirements, and it goes without saying that how critical a soluble catalyst is for decomposition of these by-products. Since the functions of RMs are determined by their intrinsic redox potentials, the current RMs are only with single or dual function, either facilitate the solution discharge process or promote the charge process. There are still no RMs that possess three functions than can simultaneously capture reactive intermediates to reduce parasitic reactions, regulate solution growth of Li_2O_2, and co-oxidize Li_2O_2 and by-products.

In this work, for the first time, we introduce a new ether class of RM, 2,5-di-tert-butyl-1,4-dimethoxybenzene (DBDMB), that can behave as an effective trifunctional soluble catalyst for boosting the performance of Li-O_2 batteries. Systematic studies have proved that DBDMB can capture Li^+ and reactive O_2^-, enabling the solution growth of large toroidal Li_2O_2 particles and avoiding the serious parasitic reactions of O_2^- towards solvent and cathode, thus giving a large discharge capacity and a high Li_2O_2 yield of 96.6%, which much higher than the usually about 80% Li_2O_2 yields of normal batteries. Moreover, the intrinsic suitable redox potential (4.20 V determined by cyclic voltammograms) of DBDMB can not only oxidize Li_2O_2 at a relatively low voltage, but also efficiently remove the main by-products, Li_2CO_3 and LiOH. DFT calculations confirm that the electron-rich nature of O atoms is the premise for DBDMB oxidation at a suitable potential, while the electronic delocalization of DBDMB and $DBDMB^+$ by p-π conjugation is the guarantee for their reversible conversion. As a result, the incorporation of DBDMB into the electrolyte increases the discharge capacity as well as contributes to long cycling stability of Li-O_2 batteries.

Results and Discussion

Redox Properties of DBDMB

The redox properties of DBDMB were determined by cyclic voltammetry (CV) measurements in a three-electrode electrochemical cell with 1 M $LiCF_3SO_3$ and 5 mM DBDMB dissolved in tetraethylene glycol dimethyl ether (TEGDME) as electrolyte. To exclude the disturbance of oxygen reduction reaction (ORR), CVs were carried out under the O_2 atmosphere in a narrow potential window of 3.8–4.5 V. As indicated in Figure 1a, DBDMB shows a redox potential of 4.20 V, which is higher than the theoretical redox potential of Li-O_2 batteries (2.96 V), so it can enable Li_2O_2 to be oxidized during the charge process. Moreover, in Figure 1b, the Randles–Sevcik plot shows a diffusion control kinetic and

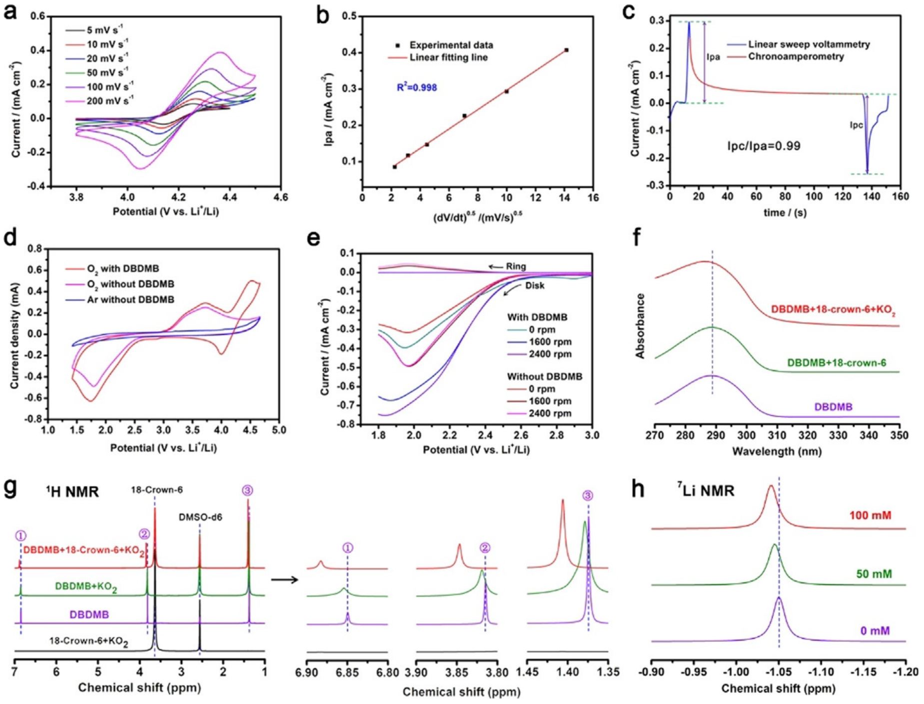

Figure 1. Cyclic voltammograms of 5 mM DBDMB in 1 M $LiCF_3SO_3$/TEGDME under O_2 atmosphere at a) various scan rates and b) corresponding Randles–Sevcik plot. c) I_{pa} and I_{pc} values determined by current transient plot of LSV (100 mVs^{-1}) and CA technologies. d) Cyclic voltammograms of electrolytes with/without 5 mM DBDMB under Ar or O_2 atmosphere at a scan rate of 50 mVs^{-1} in a wide potential window. e) RRDE test of electrolytes with/without 5 mM DBDMB at a scan rate of 100 mVs^{-1} and a ring potential of 3.5 V. f) UV/Vis and g) ^{1}H NMR spectra of DBDMB with/without O_2^-. h) ^{7}Li NMR spectra of electrolytes with different concentrations of DBDMB.

the diffusion coefficient of DBDMB is calculated to be 3.95 × 10^{-7} $cm^2 s^{-1}$. Most importantly, in Figure 1 c, the ratio of cathodic and anodic peak current (I_{pc}/I_{pa}), measured by linear sweep voltammetry (LSV) and chronoamperometry (CA), is 0.99, indicating the highly reversible redox conversion of DBDMB/DBDMB$^+$ in O_2 atmosphere, which can be further confirmed by the bare current decay in the long-term CV measurement (Supporting Information, Figure S1).

CV curves in an ORR involved potential window were also investigated (Figure 1 d). The introduction of 5 mм DBDMB into the electrolyte obviously increases the current for ORR and facilitates the process of OER, which may be attributed to the DBDMB induced solution-mediated discharge mechanism and product decomposition. To verify the discharge process follow the solution mechanism, rotating ring-disk electrode (RRDE) tests were carried out. In the electrolyte without DBDMB, the disk and ring currents remain nearly unchanged at rotation speeds of 1600 and 2400 rpm (Figure 1 e), which is accountable for the passivation of disk electrode by insulating and insoluble discharge products.[17] However, when 5 mм DBDMD is introduced, the disk current raises significantly and the ring current decreases sharply to nearly zero (Figure 1 e), indicating a solution-mediated discharge process occurs and the discharge intermediator (O_2^-) can be solvated by DBDMB. To demonstrate the capture ability of DBDMB to O_2^-, ultraviolet-visible (UV/Vis) and ^{1}H nuclear magnetic resonance (NMR) spectra were tested. As shown in Figure 1 f, the blue-shift of the maximum absorption peak of DBDMB indicates the conjugation degree of DBDMB has changed after it complexing with O_2^-. Moreover, the ^{1}H NMR spectra evidence the peak of DBDMB shift downfield (Figure 1 g), confirming that O_2^- can be captured by DBDMB. Besides, ^{7}Li NMR spectra of the electrolytes with different concentrations of DBDMB were tested. The chemical shift of ^{7}Li NMR increases with the increase of DBDMB (Figure 1 h), revealing that there is actually a strong interaction between Li^+ and DBDMB, that is, Li^+ can be solvated by DBDMB.[5a,18] On the basis of the above analysis, the solvated effect of DBDMB towards O_2^- and Li^+ is the reason for the accelerated ORR kinetic. Importantly, the CV curves experience slight change during 100 cycles (Supporting Information, Figure S2), confirming the compelling reversibility of DBDMB/DBDMB$^+$ even in the presence of strong oxidizer, Li_2O_2, O_2^-, and so on.

Functional Mechanism of DBDMB

Though a lot of RMs have been proposed in Li-O_2 batteries, their underlying functional mechanisms have been seldomly concerned. In order to unravel the inherent mechanism of DBDMB, density functional theory (DFT) calculations were carried out by Gaussian 16 software.[19] The solution-mediated discharge with DBDMB can be explained by Figure 2 a–d and the Supporting Information, Tables S1, S2. When O_2^-, Li^+, LiO_2 and Li_2O_2 complex with DBDMB, the overall Gibbs free energy changes are −3.85, −0.92, 0.01 eV and 0.21 eV, respectively, which means that DBDMB can only solvate O_2^- and Li^+, rather than LiO_2 and Li_2O_2. So we can conclude that the solvation of Li^+ and O_2^- by DBDMB is the reason for the solution discharge, which is in line with the above experimental observations. It is important that the adsorption energy of DBDMB to O_2^- is much stronger than the reported value of −0.82 eV for absorbing O_2^- on carbon cathode,[7b,20] which can avoid O_2^- induced carbon degradation and facilitate the solution growth of Li_2O_2. Moreover, DFT calculations also reveal that the complex of DBDMB:LiO_2 and DBDMB:Li_2O_2 is thermodynamically unstable, which means that when DBDMB:O_2^- further complex with Li^+ [Eq. (3)], the formation of DBDMB:LiO_2 will automatically release LiO_2 and recover DBDMB [Eq. (4)]. Finally, the released LiO_2 will disproportionate into Li_2O_2 and O_2 [Eq. (5)], and the small molecular of Li_2O_2 will tend to grow into large toroidals accompanied with the delayed passivation of cathode as well as increase of ORR current, which is consistent with our CV and RRDE observations. The Gibbs free energy changes of the above processes are shown in Figure 2 e, and the detailed discharge process can be summarized by the following equations:

$$O_2 + e^- \rightarrow O_2^- \tag{1}$$

$$O_2^- + \mathrm{DBDMB} \rightarrow \mathrm{DBDMB} : O_2^- \tag{2}$$

$$\mathrm{DBDMB} : O_2^- + Li^+ \rightarrow \mathrm{DBDMB} : LiO_2 \tag{3}$$

$$\mathrm{DBDMB} : LiO_2 \rightarrow \mathrm{DBDMB} + LiO_2 \tag{4}$$

$$2\,LiO_2 \rightarrow Li_2O_2 + O_2 \tag{5}$$

The optimized structures of DBDMB and DBDMB$^+$ are shown in Figure 2 f,h and the Supporting Information, Figure S3 and Tables S3, S4. The C, O atoms of methoxy and benzene ring are coplanar, and the bond angles of C_5-O_{10}-C_{37} (C_2-O_9-C_{41}) for DBDMB and DBDMB$^+$ are 119.3° and 121.7° respectively (approximately 120°), illustrating that the O atoms adopt sp^2 hybrid configuration. This makes the p-orbitals of O atoms perpendicular to benzene ring and parallel with their π-orbitals, and the lone pair electrons of O atoms in p-orbital partially donate to the π-orbitals of benzene ring and form p–π conjunction structure. The electronic delocalization of DBDMB is confirmed by the surface electrostatic potential map (Figure 2 g), revealing that the negative surface electrostatic potential area is mainly located on the benzene ring and O atoms. Due to the electron-rich O atoms and the nature of electronic delocalization, DBDMB will lose one electron at high oxidation potential and keep nearly identical structure except for some slight changes. As can be seen from Figure 2 f,h, when DBDMB oxidized to DBDMB$^+$, the bond length of O_{10}-C_5 (O_9-C_2) decreases from 1.37 Å to 1.32 Å, meaning that the interaction between O atoms and benzene ring is strengthened. The intensified conjugation effect is further confirmed by Mayer bond orders analysis using Multiwfn program (Supporting Information, Table S5).[21] The results show that the oxidation of DBDMB to DBDMB$^+$ makes the bond orders of O_{10}-C_5 (O_9-C_2) increase from 1.03 to 1.21, indicating that the electrons sharing between O atom and benzene ring is increased. Furthermore, the atomic charges distribution on

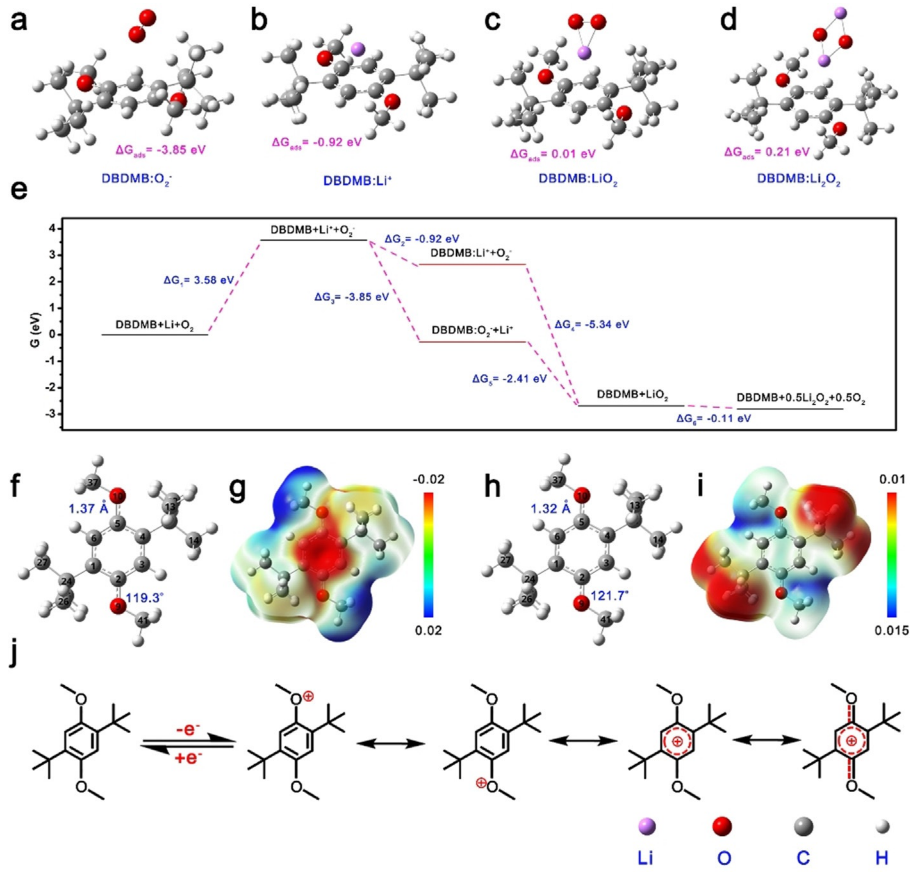

Figure 2. The optimized structures and adsorption energy of complexes a) DBDMB:O_2^-, b) DBDMB:Li^+, c) DBDMB:LiO_2, and d) DBDMB:Li_2O_2. e) The Gibbs free energy change of DBDMB, Li and O_2 at different redox states. The optimized structure of f) DBDMB and h) DBDMB$^+$. The surface electrostatic potential maps of g) DBDMB and i) DBDMB$^+$. j) The proposed resonance structures of DBDMB$^+$.

the atom of DBDMB and DBDMB$^+$ were obtained by Natural Population Analysis (NPA).[22] As shown in the Supporting Information, Table S6, when DBDMB loses one electron, the majority of positive charge discretely distributes on the O atoms and C atoms of benzene ring rather than focused on one of them, which is also confirmed by the surface electrostatic potential map of DBDMB$^+$ with the positive surface electrostatic potential area mainly located on benzene ring and O atoms (Figure 2i), and the discretely distribution of positive charge revealed by the resonance structure of DBDMB$^+$ (Figure 2j). The dispersed distribution of positive charge stabilizes DBDMB$^+$ and allows it to be reversibly reduced, as a result, long-term CV operation presents an excellent reversibility (Supporting Information, Figures S1, S2). In conclusion, the capture of Li^+ and O_2^- by the introduction of DBDMB can lead to the solution growth of Li_2O_2 and suppress the side reactions of electrolyte and electrode toward O_2^-. Moreover, we shed light on that the electron-rich O atom is the premise for the oxidation of DBDMB at suitable potential, and the effect of p–π conjunction of DBDMB and DBDMB$^+$ is the guarantee for their reversible conversion.

Discharge/Charge Behaviors of Li-O_2 Batteries with DBDMB

The discharge/charge curves of the Li-O_2 batteries with or without 50 mM DBDMB are shown in Figure 3a. It is clear that the addition of DBDMB has almost no effect on the discharge plateau (ca. 2.7 V), while plays a positive role on the charge process, decreasing the charge plateau to around 3.97 V, much lower than that of the cell without DBDMB (4.40 V). To confirm whether the introduction of DBDMB will influence the typical Li-O_2 electrochemistry or not, the cathodes at different states have been investigated by scanning electron microscopy (SEM), X-ray diffraction (XRD) and Fourier transform infrared spectroscopy (FTIR) measurements. As shown in Figure 3b and the Supporting Information, Figures S4, S5, after discharge, toroidals with sizes around 200 nm are homogeneously distributed on the porous cathode and can be identified as Li_2O_2 by XRD and FTIR. The subsequent recharge process renders the complete decomposition of Li_2O_2 toroidals, and thus the cathode recovers to its original morphology. These results certify that DBDMB does not change the electrochemical reactions of Li-O_2 batteries and permits highly reversible formation and decomposition of Li_2O_2. In combination of the above CV results, the catalytic behavior of DBDMB towards Li_2O_2 can be described as follows: on charging, DBDMB is first

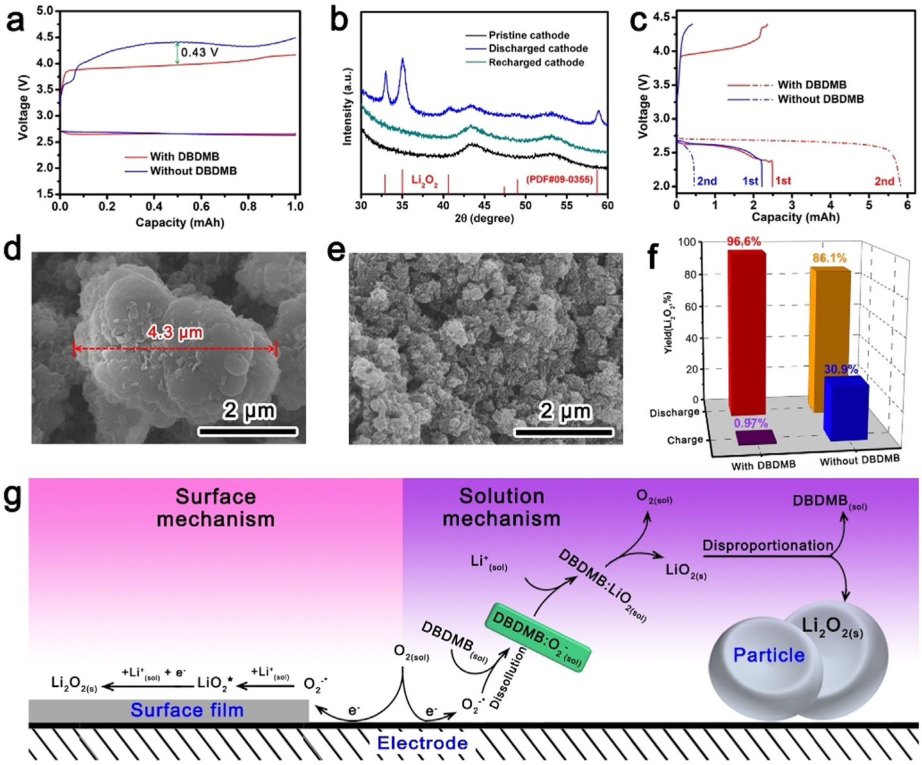

Figure 3. Discharge–charge curves of Li-O_2 batteries at a current density of 200 mAg^{-1} with a) capacity limitation of 1 mAh and c) voltage limitation of 2.0–4.4 V. b) XRD patterns of pristine, discharged and recharged cathodes with 50 mM DBDMB. SEM images of the cathodes after the 2nd full discharge to the cut-off voltage of 2.0 V d) with DBDMB and e) without DBDMB. f) The yield of Li_2O_2 determined by $TiOSO_4$-based UV/Vis spectroscopic titration with the discharge/charge capacity of 1 mAh. g) Illustration of the different Li_2O_2 growth pathways: surface mechanism and solution mechanism.

oxidized to $DBDMB^+$ at the cathode, then $DBDMB^+$ diffuses to the vicinity of Li_2O_2 particles and chemically oxidizes Li_2O_2 with the simultaneous recovery of $DBDMB^+$ to its reduced form, DBDMB. These processes continuously happen until all Li_2O_2 entirely decompose.

The superior capability of DBDMB towards catalytic oxidation of Li_2O_2 can be further confirmed by the full discharge/charge curves of Li-O_2 batteries with/without DBDMB (Figure 3c). Since the Li-O_2 batteries used identical cathodes and anodes, the relative larger discharge capacity of the one with DBDMB can be attributed to its solvation of Li^+ and O_2^- induced solution growth of Li_2O_2 (Figure 3g), which has been demonstrated by above experimental observations and DFT calculations. The solution discharge process is further evidenced by the formation of large, red-blood-cell-like Li_2O_2 toroidals with diameters of about 600 nm in the cell with DBDMB (Supporting Information, Figure S6a), being different from the small flake-type Li_2O_2 formed on the cell without DBDMB (Supporting Information, Figure S6b). Moreover, the reversible capacity of the cell with DBDMB is almost the same as the full discharge capacity (Figure 3c), indicating that DBDMB can efficiently catalyze Li_2O_2 decomposition even at a deep discharge state. In stark contrast, the charge capacity of Li-O_2 battery without DBDMB is much lower than the discharge capacity due to the loss of close contact between the cathode and Li_2O_2. The undecomposed Li_2O_2 will passivate the cathode by burying the electrochemically active sites, which in turn seriously reduces the second discharge capacity (Figure 3c). With regard to the cell with DBDMB, instead of damping, the second discharge capacity doubles (two times of the first discharge capacity) along with the formation of particle-type Li_2O_2 with diameters up to 4–5 μm (Figure 3d; Supporting Information, Figure S7). While for the cell without DBDMB, the size of the flake-type Li_2O_2 is even smaller than that of the 1st discharge cycle (Figure 3e), in line with the much smaller 2nd discharge capacity than the first one. The capacity increase phenomenon for the cell with DBDMB has never been reported before. The most possible reason is described as follows: the original structure of the cathode full of active sites is almost recovered after the first charge process, but there is still a small fraction of Li_2O_2 inevitably remaining due to the limitation of charge voltage. These residual Li_2O_2 can behave as seed crystals to allow solvated Li_2O_2 to nucleate on their surfaces and grow into large particles with greatly enhanced capacity.

The capture of reactive O_2^- by DBDMB can avoid the related parasitic reactions. To confirm this, the yield of Li_2O_2 for the two cells with the same discharge/charge capacity of 1 mAh was determined by $TiOSO_4$-based UV/Vis spectroscopic titration (Figure 3f; Supporting Information, Figure S8). The battery with DBDMB exhibits a high Li_2O_2 generation efficiency of 96.6% and an extremely low residual rate of 0.97% after subsequent recharge process. However,

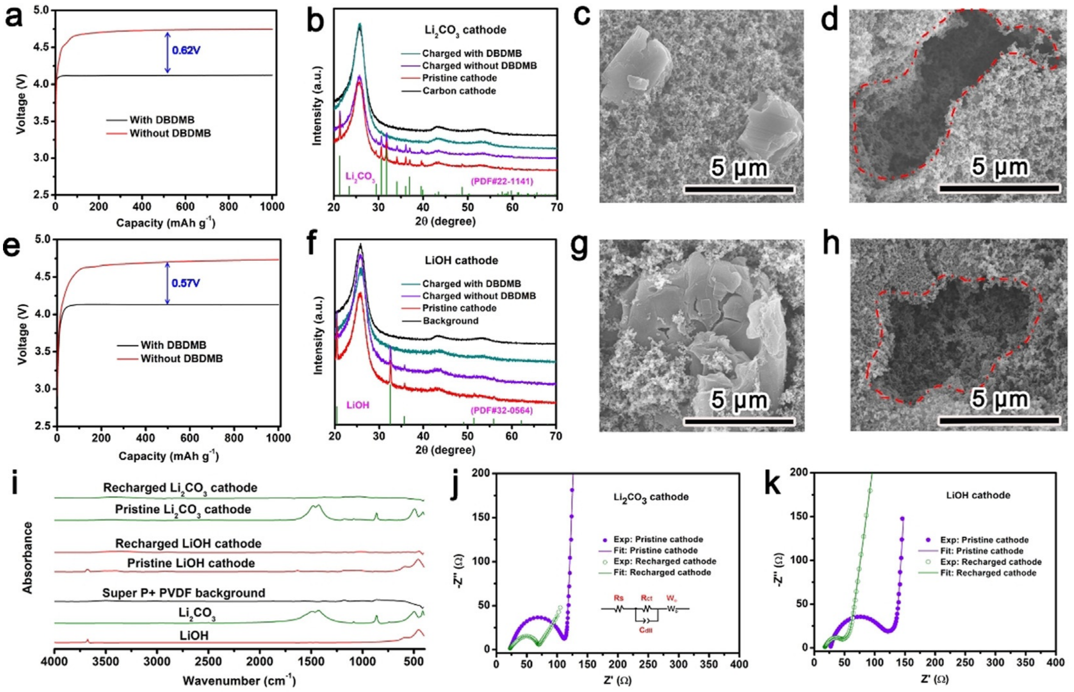

Figure 4. Charge profiles of the cathodes pre-loaded with a) Li_2CO_3 and e) LiOH with/without DBDMB at a limited capacity of 1000 mAh g^{-1} and a current density of 200 mA g^{-1}. XRD patterns of the pristine and recharged b) Li_2CO_3 and f) LiOH pre-loaded cathodes with/without DBDMB. SEM images of the pristine c) Li_2CO_3 and g) LiOH pre-loaded cathodes, and the corresponding recharged d) Li_2CO_3 and h) LiOH pre-loaded cathodes with DBDMB. i) FTIR spectra of the pristine/recharged Li_2CO_3 and LiOH pre-loaded cathodes. Nyquist plots of the EIS data of the pristine/recharged j) Li_2CO_3 and k) LiOH pre-loaded cathodes with DBDMB.

the battery without DBDMB shows a relatively lower Li_2O_2 generation efficiency of 86.1 % and a much higher residual rate of 30.9 %. Less parasitic reaction products can also be proved by the ^{1}H NMR spectra in the Supporting Information, Figure S9, which point out that a much lower content of CH_3COOLi by-product has been formed in the cell with DBDMB. Meanwhile, the homogenous and efficient catalytic ability of DBDMB makes the cell show a low Li_2O_2 residual rate of 0.97 %, which not only facilitates the cathode to recover to its original state, but also leaves small Li_2O_2 crystals to act as nucleating centers for promoting solvated Li_2O_2 to grow into large particles together with a high discharge capacity. Previously, the design of RMs was only focused on facilitating the formation and decomposition of Li_2O_2, no one has ever reported that a RM can capture O_2^- to reduce parasitic reaction products.

Catalytic Ability of DBDMB towards Li_2CO_3 and LiOH

The higher redox potential of DBDMB (4.20 V) than those of Li_2CO_3 and LiOH (3.82 and 3.39 V),[9g,23] make it may possess the ability to oxidize decomposition of these main parasitic products for Li-O_2 batteries. To verify this, the cathodes pre-loaded with commercial Li_2CO_3 and LiOH were prepared with mass loading restricted to 1000 mAh g$^{-1}_{\text{carbon}}$. As indicated in Figure 4 a,e, with the help of 200 mM DBDMB, the cathodes pre-loaded with Li_2CO_3 and LiOH can be recharged to the pre-loaded capacity at the voltage plateaus of 4.12 V and 4.13 V, respectively, much lower than those of the charge plateaus of normal batteries (4.74 and 4.70 V), which with similar values reported by other groups.[24] To determine whether these Li_2CO_3 or LiOH particles are removed or not, XRD patterns and SEM images of the cathodes at different states were investigated. From Figure 4 b,f, we can see that there are still some residual peaks corresponding to Li_2CO_3 and LiOH existing when the cathodes are charged without DBDMB, in accordance with the observation of the remain of large particles in the recharged cathodes (Supporting Information, Figure S10). However, when the cathodes are charged with DBDMB, none Li_2CO_3 and LiOH peaks and particles can be observed (Figure 4 b,d,f,h), except leaves several micron hollow pits in the recharged cathodes, revealing that the introduction of DBDMB can overcome the high intrinsic barrier for oxidizing redox-inert anions, CO_3^{2-} and OH^- and permit the decomposition of Li_2CO_3 and LiOH at low voltages, thus avoiding the high charge voltage induced degradation of glyme-based electrolyte and prolonging the battery lifetime.[24b,25] The catalytic activity of DBDMB towards Li_2CO_3 and LiOH has also been evidenced by FTIR spectra with the disappearance of the characteristic IR absorbance peaks of Li_2CO_3 and LiOH after recharging (Figure 4 i). Electrochemical impedance spectra (EIS) further confirm the catalytic Li_2CO_3 and LiOH decomposition ability of DBDMB (Figure 4 j,k; Supporting Information, Figure S11 and Table S7). The schematic illustration of the DBDMB assisted oxidative decomposition of Li_2O_2, LiOH and Li_2CO_3 in Li-O_2 batteries is shown in

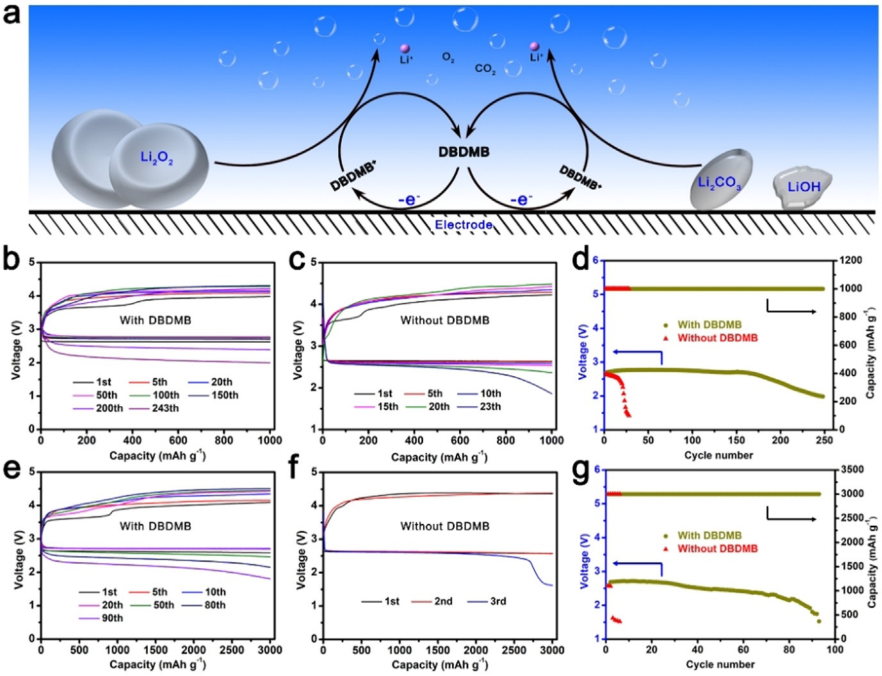

Figure 5. a) Illustration of the oxidization reaction mechanism of DBDMB towards Li_2O_2, LiOH, and Li_2CO_3 in Li-O_2 batteries. Cycling performance of the Li-O_2 batteries with/without DBDMB with a capacity limitation of b)–d) 1000 mAh g^{-1} and e)–g) 3000 mAh g^{-1} at a current density of 1000 mA g^{-1}.

Figure 5a. This is the first RM that can simultaneously promote the charge process by co-decomposing Li_2O_2, Li_2CO_3 and LiOH, and boost the discharge process by capturing O_2^-, demonstrating the trifunctional ability of our DBDMB.

Cycling Performance of Li-O_2 Batteries with DBDMB

With the help of experimental observations and DFT calculations, we can know that the incorporation of DBDMB can facilitate the solution discharge mechanism and reduce the formation of parasitic reaction products (Li_2CO_3 and LiOH) by capturing the reactive O_2^-, as well as promote almost full recovery of the active sites of cathode by efficiently co-decomposing Li_2O_2 and by-products, fulfilling all the strictest requirements for enabling Li-O_2 batteries to deliver a long cycling life. Therefore, the cycling performance of Li-O_2 batteries with/without DBDMB was tested to confirm this. As shown in Figure 5b–d, the battery with 200 mM DBDMB presents a long cycle lifetime of 243 cycles at a high current density of 1000 mA g^{-1} with a capacity limitation of 1000 mAh g^{-1} (Figure 5b), more than 10 times the lifespan of the battery without DBDMB (Figure 5c,d). Furthermore, even at a higher cut-off capacity of 3000 mAh g^{-1}, the cell with DBDMB can still normally run for 90 cycles, 30 times than that of the cell without DBDMB (Figure 5e–g), indicating that the DBDMB exactly plays positive roles on boosting the lifetime of Li-O_2 batteries and can satisfy the fast charge transfer kinetics requirement for cycling Li-O_2 batteries at large rates and capacities.

Conclusion

We have shown that DBDMB, a new class of ether-based redox mediator, is an effective trifunctional liquid catalyst for increasing the discharge capacity and prolonging the cycling stability of Li-O_2 batteries. With the addition of DBDMB, its strong adsorption ability toward Li^+ and O_2^- promotes the solution growth of Li_2O_2 and avoids the reactive O_2^- induced parasitic reactions, thus, a large discharge capacity and a high Li_2O_2 yield of 96.6% are realized. Furthermore, the suitable redox potential of DBDMB (4.20 V) can not only oxidize Li_2O_2 easily, but also facilitate the decomposition of the main by-products (Li_2CO_3 and LiOH) of Li-O_2 batteries, which together enable the recovery of the active sites of cathode and contribute to a prolonged cycling stability. The detailed functional mechanisms of DBDMB have also been revealed by DFT calculations, which can help us comprehensively understand the system and carry out future in-depth research. The strategy of reducing parasitic reactions, and co-oxidizing Li_2O_2 and by-products (Li_2CO_3 and LiOH) through introducing a solvating redox mediator will open a new door to boost the performance of Li-air batteries.

Acknowledgements

This work was financially supported by the National Key R&D Program of China (2017YFA0206700), the National Natural Science Foundation of China (21725103, 51702314), the Strategic Priority Research Program of the Chinese Academy of Sciences (XDA21010210), the Jilin Province Science and Technology Development Plan Funding Project

(20180101203JC), the K. C. Wong Education Foundation (GJTD-2018-09), the Changchun Science and Technology Development Plan Funding Project (19SS010) and the National & local united engineering lab for power battery. The Supercomputing USTC is acknowledged for computational support.

Conflict of interest

The authors declare no conflict of interest.

Keywords: 2,5-di-tert-butyl-1,4-dimethoxybenzene · DFT calculations · redox mediators · solution mechanism · trifunctional mediators

---

[1] a) K. M. Abraham, Z. Jiang, *J. Electrochem. Soc.* **1996**, *143*, 1–5; b) T. Ogasawara, A. Debart, M. Holzapfel, P. Novak, P. G. Bruce, *J. Am. Chem. Soc.* **2006**, *128*, 1390–1393.

[2] a) Z. Peng, S. A. Freunberger, Y. Chen, P. G. Bruce, *Science* **2012**, *337*, 563–566; b) D. Aurbach, B. D. McCloskey, L. F. Nazar, P. G. Bruce, *Nat. Energy* **2016**, *1*, 16128; c) T. Liu, X.-L. Feng, X. Jin, M.-Z. Shao, Y.-T. Su, Y. Zhang, X.-B. Zhang, *Angew. Chem. Int. Ed.* **2019**, *58*, 18240–18245; *Angew. Chem.* **2019**, *131*, 18408–18413; d) C. Xia, C. Y. Kwok, L. F. Nazar, *Science* **2018**, *361*, 777–781; e) J. L. Ma, F. L. Meng, Y. Yu, D. P. Liu, J. M. Yan, Y. Zhang, X. B. Zhang, Q. Jiang, *Nat. Chem.* **2019**, *11*, 64–70; f) Z. Zhu, X. Shi, G. Fan, F. Li, J. Chen, *Angew. Chem. Int. Ed.* **2019**, *58*, 19021–19026; *Angew. Chem.* **2019**, *131*, 19197–19202; g) M. Asadi, B. Sayahpour, P. Abbasi, A. T. Ngo, K. Karis, J. R. Jokisaari, C. Liu, B. Narayanan, M. Gerard, P. Yasaei, X. Hu, A. Mukherjee, K. C. Lau, R. S. Assary, F. Khalili-Araghi, R. F. Klie, L. A. Curtiss, A. Salehi-Khojin, *Nature* **2018**, *555*, 502–506; h) G. Cong, W. Wang, N. C. Lai, Z. Liang, Y. C. Lu, *Nat. Mater.* **2019**, *18*, 390–396; i) X.-Y. Yang, X.-L. Feng, X. Jin, M.-Z. Shao, B.-L. Yan, J.-M. Yan, Y. Zhang, X.-B. Zhang, *Angew. Chem. Int. Ed.* **2019**, *58*, 16411–16415; *Angew. Chem.* **2019**, *131*, 16563–16567; j) Z. Zhang, S. Wu, C. Yang, L. Zheng, D. Xu, R. Zha, L. Tang, K. Cao, X. G. Wang, Z. Zhou, *Angew. Chem. Int. Ed.* **2019**, *58*, 17782–17787; *Angew. Chem.* **2019**, *131*, 17946–17951.

[3] a) N. B. Aetukuri, B. D. McCloskey, J. M. Garcia, L. E. Krupp, V. Viswanathan, A. C. Luntz, *Nat. Chem.* **2015**, *7*, 50–56; b) A. C. Luntz, V. Viswanathan, J. Voss, J. B. Varley, J. K. Nørskov, R. Scheffler, A. Speidel, *J. Phys. Chem. Lett.* **2013**, *4*, 3494–3499.

[4] a) F. Tian, M. D. Radin, D. J. Siegel, *Chem. Mater.* **2014**, *26*, 2952–2959; b) O. Gerbig, R. Merkle, J. Maier, *Adv. Mater.* **2013**, *25*, 3129–3133.

[5] a) C. M. Burke, V. Pande, A. Khetan, V. Viswanathan, B. D. McCloskey, *Proc. Natl. Acad. Sci. USA* **2015**, *112*, 9293–9298; b) D. Sharon, D. Hirsberg, M. Salama, M. Afri, A. A. Frimer, M. Noked, W. Kwak, Y. K. Sun, D. Aurbach, *ACS Appl. Mater. Interfaces* **2016**, *8*, 5300–5307.

[6] a) Y. Qiao, S. Wu, J. Yi, Y. Sun, S. Guo, S. Yang, P. He, H. Zhou, *Angew. Chem. Int. Ed.* **2017**, *56*, 4960–4964; *Angew. Chem.* **2017**, *129*, 5042–5046; b) X. Gao, Z. P. Jovanov, Y. Chen, L. R. Johnson, P. G. Bruce, *Angew. Chem. Int. Ed.* **2017**, *56*, 6539–6543; *Angew. Chem.* **2017**, *129*, 6639–6643.

[7] a) X. Gao, Y. Chen, L. Johnson, P. G. Bruce, *Nat. Mater.* **2016**, *15*, 882–888; b) Y. Zhang, L. Wang, X. Zhang, L. Guo, Y. Wang, Z. Peng, *Adv. Mater.* **2018**, *30*, 1705571; c) Y. Ko, H. Park, J. Kim, H. D. Lim, B. Lee, G. Kwon, S. Lee, Y. Bae, S. K. Park, K. Kang, *Adv. Funct. Mater.* **2019**, *29*, 1805623; d) P. Zhang, L. Liu, X. He, X. Liu, H. Wang, J. He, Y. Zhao, *J. Am. Chem. Soc.* **2019**, *141*, 6263–6270.

[8] J. Wang, Y. Zhang, L. Guo, E. Wang, Z. Peng, *Angew. Chem. Int. Ed.* **2016**, *55*, 5201–5205; *Angew. Chem.* **2016**, *128*, 5287–5291.

[9] a) Y. Chen, S. A. Freunberger, Z. Peng, O. Fontaine, P. G. Bruce, *Nat. Chem.* **2013**, *5*, 489–494; b) D. Sun, Y. Shen, W. Zhang, L. Yu, Z. Yi, W. Yin, D. Wang, Y. Huang, J. Wang, D. Wang, J. B. Goodenough, *J. Am. Chem. Soc.* **2014**, *136*, 8941–8946; c) B. J. Bergner, A. Schurmann, K. Peppler, A. Garsuch, J. Janek, *J. Am. Chem. Soc.* **2014**, *136*, 15054–15064; d) Q. Zhao, N. Katyal, I. D. Seymour, G. Henkelman, T. Ma, *Angew. Chem. Int. Ed.* **2019**, *58*, 12553–12557; *Angew. Chem.* **2019**, *131*, 12683–12687; e) D. Kundu, R. Black, B. Adams, L. F. Nazar, *ACS Cent. Sci.* **2015**, *1*, 510–515; f) Z. Liang, Y. C. Lu, *J. Am. Chem. Soc.* **2016**, *138*, 7574–7583; g) W.-J. Kwak, D. Hirshberg, D. Sharon, M. Afri, A. A. Frimer, H.-G. Jung, D. Aurbach, Y.-K. Sun, *Energy Environ. Sci.* **2016**, *9*, 2334–2345; h) Y. Ko, H. Park, K. Lee, S. J. Kim, H. Park, Y. Bae, J. Kim, S. Y. Park, J. E. Kwon, K. Kang, *Angew. Chem. Int. Ed.* **2020**, *59*, 5376–5380; *Angew. Chem.* **2020**, *132*, 5414–5418.

[10] R. Black, J. H. Lee, B. Adams, C. A. Mims, L. F. Nazar, *Angew. Chem. Int. Ed.* **2013**, *52*, 392–396; *Angew. Chem.* **2013**, *125*, 410–414.

[11] N. Feng, P. He, H. Zhou, *Adv. Energy Mater.* **2016**, *6*, 1502303.

[12] a) R. S. Assary, J. Lu, P. Du, X. Luo, X. Zhang, Y. Ren, L. A. Curtiss, K. Amine, *ChemSusChem* **2013**, *6*, 51–55; b) S. A. Freunberger, Y. Chen, N. E. Drewett, L. J. Hardwick, F. Barde, P. G. Bruce, *Angew. Chem. Int. Ed.* **2011**, *50*, 8609–8613; *Angew. Chem.* **2011**, *123*, 8768–8772.

[13] a) R. Younesi, M. Hahlin, F. Björefors, P. Johansson, K. Edström, *Chem. Mater.* **2013**, *25*, 77–84; b) B. D. McCloskey, A. Speidel, R. Scheffler, D. C. Miller, V. Viswanathan, J. S. Hummelshoj, J. K. Norskov, A. C. Luntz, *J. Phys. Chem. Lett.* **2012**, *3*, 997–1001.

[14] a) J. J. Xu, Q. C. Liu, Y. Yu, J. Wang, J. M. Yan, X. B. Zhang, *Adv. Mater.* **2017**, *29*, 1606552; b) B. D. McCloskey, A. Valery, A. C. Luntz, S. R. Gowda, G. M. Wallraff, J. M. Garcia, T. Mori, L. E. Krupp, *J. Phys. Chem. Lett.* **2013**, *4*, 2989–2993; c) B. Zhou, L. Guo, Y. Zhang, J. Wang, L. Ma, W. H. Zhang, Z. Fu, Z. Peng, *Adv. Mater.* **2017**, *29*, 1701568.

[15] M. M. Ottakam Thotiyl, S. A. Freunberger, Z. Peng, P. G. Bruce, *J. Am. Chem. Soc.* **2013**, *135*, 494–500.

[16] C. Ling, R. Zhang, K. Takechi, F. Mizuno, *J. Phys. Chem. C* **2014**, *118*, 26591–26598.

[17] D. G. Kwabi, M. Tulodziecki, N. Pour, D. M. Itkis, C. V. Thompson, Y. Shao-Horn, *J. Phys. Chem. Lett.* **2016**, *7*, 1204–1212.

[18] C. Chen, X. Chen, X. Zhang, L. Li, C. Zhang, T. Huang, A. Yu, *J. Mater. Chem. A* **2018**, *6*, 7221–7226.

[19] G. W. T. M. J. Frisch, H. B. Schlegel, G. E. Scuseria, M. A. Robb, J. R. Cheeseman, G. Scalmani, V. Barone, G. A. Petersson, H. Nakatsuji, X. Li, M. Caricato, A. V. Marenich, J. Bloino, B. G. Janesko, R. Gomperts, B. Mennucci, H. P. Hratchian, J. V. Ortiz, A. F. Izmaylov, J. L. Sonnenberg, D. Williams-Young, F. Ding, F. Lipparini, F. Egidi, J. Goings, B. Peng, A. Petrone, T. Henderson, D. Ranasinghe, V. G. Zakrzewski, J. Gao, N. Rega, G. Zheng, W. Liang, M. Hada, M. Ehara, K. Toyota, R. Fukuda, J. Hasegawa, M. Ishida, T. Nakajima, Y. Honda, O. Kitao, H. Nakai, T. Vreven, K. Throssell, J. A. Montgomery, Jr., J. E. Peralta, F. Ogliaro, M. J. Bearpark, J. J. Heyd, E. N. Brothers, K. N. Kudin, V. N. Staroverov, T. A. Keith, R. Kobayashi, J. Normand, K. Raghavachari, A. P. Rendell, J. C. Burant, S. S. Iyengar, J. Tomasi, M. Cossi, J. M. Millam, M. Klene, C. Adamo, R. Cammi, J. W. Ochterski, R. L. Martin, K. Morokuma, O. Farkas, J. B. Foresman, D. J. Fox, Gaussian, Inc., Wallingford CT **2016**.

[20] J. J. Xu, Z. W. Chang, Y. Wang, D. P. Liu, Y. Zhang, X. B. Zhang, *Adv. Mater.* **2016**, *28*, 9620–9628.

[21] a) T. Lu, F. Chen, *J. Comput. Chem.* **2012**, *33*, 580–592; b) I. Mayer, *Chem. Phys. Lett.* **1983**, *97*, 270–274; c) I. Mayer, *Int. J. Quantum Chem.* **1984**, *26*, 151–154.

[22] a) A. E. Reed, R. B. Weinstock, F. Weinhold, *J. Chem. Phys.* **1985**, *83*, 735–746; b) T. Lu, F. Chen, *Acta Phys. Chim. Sin.* **2012**, *28*, 1–18.

[23] P. Tan, Z. H. Wei, W. Shyy, T. S. Zhao, X. B. Zhu, *Energy Environ. Sci.* **2016**, *9*, 1783–1793.

[24] a) S. Yang, P. He, H. Zhou, *Energy Environ. Sci.* **2016**, *9*, 1650–1654; b) S. Meini, N. Tsiouvaras, K. U. Schwenke, M. Piana, H. Beyer, L. Lange, H. A. Gasteiger, *Phys. Chem. Chem. Phys.* **2013**, *15*, 11478–11493.

[25] a) D. Geng, N. Ding, T. S. Hor, S. W. Chien, Z. Liu, Y. Zong, *Chem. Asian J.* **2015**, *10*, 2182–2189; b) H. Beyer, S. Meini, N. Tsiouvaras, M. Piana, H. A. Gasteiger, *Phys. Chem. Chem. Phys.* **2013**, *15*, 11025–11037.

Manuscript received: June 30, 2020
Accepted manuscript online: July 21, 2020
Version of record online: August 26, 2020